Hydrothermal Degassing Through the Karakoram Fault, Western Tibet: Insights Into Active Deformation Driven by Continental Strike-Slip Faulting

Maoliang Zhang[1,*], Xian-Gang Xie[1], Wei Liu[2], Yi Liu[1], Linan Wang[1], Yuji Sano[3,4], Yun-Chao Lang[1], Cong-Qiang Liu[1], and Sheng Xu[1,*]

[1]School of Earth System Science, Tianjin University, Tianjin 300072, China.

[2]College of Resources and Environmental Engineering, Inner Mongolia University of Technology, Hohhot 010051, China.

[3]Marine Core Research Institute, Kochi University, Kochi 783-8502, Japan.

[4]Atmosphere and Ocean Research Institute, The University of Tokyo, Chiba 277-8564, Japan.

*Corresponding author:

Maoliang Zhang (mzhang@tju.edu.cn) and Sheng Xu (sheng.xu@tju.edu.cn)

Key Points:

- New He isotope data show that southern Karakoram fault is overwhelmingly dominated by degassing of crustal fluids
- A crustal ^{4}He- and CO_2-rich fluid reservoir is identified and linked to crustal-scale active deformation driven by strike-slip faulting
- Karakoram fault may have limited fluid connections to the mantle and requires further evaluation based on He isotope and seismic data

Abstract

The Karakoram fault is an important strike-slip boundary for accommodating deformation following the India-Asia collision. However, whether the deformation is confined to the crust or whether it extends into the mantle remains highly debated. Here, we show that the Karakoram fault is overwhelmingly dominated by crustal degassing related to a ^{4}He- and CO_2-rich fluid reservoir [e.g., He contents up to ~1.0−1.6 vol.%; $^{3}He/^{4}He$ = 0.029 ± 0.016 R_A (1σ, n = 50); CO_2/N_2 up to 3.7−57.8]. Crustal-scale active deformation driven by strike-slip faulting could mobilize ^{4}He and CO_2 from the fault zone rocks, which subsequently accumulate in the hydrothermal system. The Karakoram fault may have limited fluid connections to the mantle, and if any, the accumulated crustal fluids would efficiently dilute the uprising mantle fluids. In both cases, crustal deformation is evidently the first-order response to strike-slip faulting.

Plain Language Summary

Bubbling hot springs are common in fault zones along which Earth's lithosphere cracks. Chemical and isotopic compositions of spring gases can offer key information on the subsurface connectivity of the deep-rooting faults that is not easily visible. To assess whether the Karakoram fault in western Tibetan Plateau is developing in the crust or extends into deeper mantle, we studied the origin and transport of spring gases and found that the Karakoram fault is overwhelmingly dominated by degassing of a crustal fluid reservoir that contains high amounts of helium (He) and CO_2. This could be attributed to He-CO_2 mobilization of deforming and fracturing fault zone rocks at crustal depths, suggesting that the Karakoram fault is primarily developing in the crust and may have limited fluid connections to the mantle.

1. Introduction

Continent-continent collision between India and Asia, as documented by the Himalayan-Tibetan orogen, resulted in shortening and extrusion of the lithosphere over vast distances (Ding et al., 2022). Whether the India-Asia collision is characterized by deformation confined to crustal depths, or alternatively, reaching the underlying mantle lithosphere, holds the key for unraveling the dynamics of orogenic plateau growth driven by the forces acting on the colliding continents (Copley et al., 2011; Royden et al., 2008). Strike-slip faults are likely to penetrate through brittle-ductile transition zone and offset the Moho (Bourne et al., 1998; Sylvester, 1988), thus providing a window for gaining insights into the collision-driven deformation from mantle to crustal depths. Therefore, the depth extent of strike-slip faults is a key parameter in modeling outward growth of the Tibetan Plateau in response to India-Asia collision.

The right-lateral Karakoram fault (KKF) extends >1000 km from the Pamir to western Himalayas (Figure 1a), serving as an important plate boundary to accommodate shortening and modulate eastward extrusion of the Tibetan Plateau (Chevalier et al., 2015). The depth extent of the KKF penetration and deformation is still debated between kinematic models in favor of either crustal- or lithospheric-scale strike-slip faulting (Leech, 2008; Searle & Phillips, 2007; Van Buer et al., 2015). As the KKF exhibits geometrical segmentation (inset in Figure 1b) and varies in kinematics among different fault segments (Robinson et al., 2015), shear deformation may have heterogeneity along its strike. Such along-strike deformation has been examined for the geological past by field observations and evidence from metamorphism, magmatism, geochronology, and slip rate reconstruction (Chevalier, 2019; Searle & Phillips, 2007; Wallis et al., 2013). However, what remains challenging is that how underlying active deformation could be constrained by modern observations at the surface. GPS-based geodetic measurements have

been used to establish strain partitioning patterns and active deformation of the KKF and adjacent regions (Wright et al., 2004), but surface strain rates may be less informative for inferring whether the deforming layer extends into the mantle or whether it ends within the crust (Royden et al., 2008).

An alternative approach for constraining active deformation at depth is the geochemistry of hydrothermal fluids (e.g., thermal spring gases and waters), which is sensitive to tectonic and physical processes in the deep-rooting fault zones (Rosen et al., 2018). In particular, integrating geochemical data with geophysical observations (Gao et al., 2016) could provide unique insights into underlying structure and active deformation. Previous studies have identified mantle fluids in thermal springs and suggested that the depth extent of the KKF could reach lithospheric mantle (Bai et al., 2023; Hoke et al., 2000; Klemperer et al., 2013). Notably, only two out of nineteen geothermal fields on and off the KKF show unequivocal mantle fluids (Klemperer et al., 2013): Menshi [referred to as Tirthapuri in Hoke et al. (2000)] on the KKF, and Langjiu [referred to as Shiquanhe in Hoke et al. (2000)] ~45 km off the KKF to the NE (Figure 1a; see details in *Section 2.2*). Zooming out from Menshi and Langjiu, it becomes evident that the KKF is long and has several segments. From a geochemical point of view, our understanding of hydrothermal degassing remains limited to constrain segmental characteristics of active deformation beneath the KKF.

In this study, we focus on the origin and transport of deeply-sourced volatiles (e.g., He and CO_2) released by thermal springs on and off the southern KKF (Figure 1b; northern KKF is almost inaccessible for political reasons), aiming to provide new insights into active deformation driven by strike-slip faulting in western Tibetan Plateau. Our new He isotope data indicate that the KKF is dominated by crustal degassing both on and off its southern segments. A crustal ^{4}He-

and CO_2-rich fluid reservoir is identified in the subsurface hydrothermal systems, which could be attributed to crustal-scale active deformation that liberates large amounts of ^4He and CO_2 from deforming and fracturing fault zone rocks. We further examined mantle-to-crust fluid connections of the KKF and the dilution effects of crustal ^4He-rich fluids based on regional seismic data.

2. Materials and Methods

2.1. Sample Distribution and Laboratory Analysis

We adopted geometrical segmentation of the KKF (inset in Figure 1b; Chevalier et al., 2015) to describe sample distribution. Seventeen free gas samples were collected from thermal springs along the Gar and Menshi-Kailas segments, as well as the Langjiu geothermal field off the KKF (Figure 1a). Due to the limits by transportation conditions and accessibility factors, we were unable to collect samples from other fault segments. For example, the K2 segment (i.e., northern KKF; Figure 1b) and Bangong-Chaxikang segment are barely accessible due to their closeness to the politically unstable Kashmir and China-India border. Chemical and isotopic compositions (e.g., $^3He/^4He$ and $\delta^{13}C\text{-}CO_2$) of hydrothermal gases were analyzed as soon as possible to avoid post-sampling air contamination. Details of field campaign, sampling procedures, analytical methods, and geochemical data are given in Text S1 and Table S1 of the Supporting Information S1.

2.2. Helium Isotope Systematics and Data Compilation

Helium isotope ratio [$^3He/^4He$ (R) reported relative to R_A, where R_A = air $^3He/^4He = 1.39 \times 10^{-6}$] of modern hydrothermal fluids is a unique tracer for quantifying the mixing between crustal and mantle fluids that possibly occurs in active fault zones (Caracausi et al., 2022; Sano

& Fischer, 2013; Umeda & Ninomiya, 2009). The convective upper mantle, i.e., source of mid-ocean ridge basalts (MORB), has an uniform $^{3}He/^{4}He$ ratio of 8 ± 1 R_A (Graham, 2002), while that of the sub-continental lithospheric mantle (SCLM) is lower (6.1 ± 2.1 R_A; Day et al., 2015). In contrast, the continental crust has accumulated large amounts of radiogenic ^{4}He due to U-Th decay through time, yielding significantly low $^{3}He/^{4}He$ ratios such as 0.02 R_A (Andrews, 1985). Variable amounts of atmospheric He could be detected in the sample due to recharge of air-saturated water (ASW) into hydrothermal systems and post-sampling contamination. As such, the measured $^{3}He/^{4}He$ must be corrected assuming that all ^{20}Ne in the sample is derived from ASW (Craig et al., 1978).

A reference X value of ~10, where $X = (He/Ne)_{sample}/(He/Ne)_{air} \times \beta_{Ne}/\beta_{He}$, was used to rule out data showing significant air contamination (Klemperer et al., 2022; Zhang et al., 2021a). Our He isotope data are in high quality with <1% ASW-derived He (Figure 2). In addition, He isotope data in literature were compiled and classified into the following groups: On-KKF (K2), On-KKF (Gar), On-KKF (Menshi-Kailas), Off-KKF, western Lhasa block, and western Himalayas (Data Set S1 in Supporting Information S1). Among them, six low X-value (mostly <10) samples from four geothermal fields (i.e., Menshi, Changlung, Duoguoqu, and Xiongbacun) on the K2 and Menshi-Kailas segments were excluded from discussion. In particular, Changlung (Klemperer et al., 2013) and Duoguoqu (Bai et al., 2023) were suggested to discharge mantle fluids but were not considered in this study due to uncertain data quality (Figure 2). To assess whether unequivocal mantle fluids are releasing at Changlung and Duoguoqu, new He isotope measurements need to be conducted in future; but this possibility does not impact our discussion and conclusion.

Spatially, most samples are distributed on and off the Gar and Menshi-Kailas segments, and four samples from Klemperer et al. (2013, 2022) are ~40−60 km off the Bangong-Chaxikang segment (Figure 1). In addition, considering the lack of detailed field work to confirm the affinity of the Kailas-Thakkhola segment to the KKF (Chevalier, 2019), our newly acquired data, along with the compiled literature data, would be suitable for constraining hydrothermal degassing from the southern KKF, including the Bangong-Chaxikang, Gar, and Menshi-Kailas segments.

3. Results and Discussion

3.1. Regional $^3He/^4He$ Variability and Possible Temporal Changes

There is a general consensus that any air-corrected $^3He/^4He$ ratio (R_C) higher than 0.1 R_A (>1% mantle He inputs assuming 8 R_A for the mantle and 0.02 R_A for the crust) is considered unambiguous evidence for mantle degassing (Crossey et al., 2009), i.e., fluid connections to the mantle. Conversely, those lower than 0.1 R_A represent crustal degassing. All our samples (R_C = 0.015−0.042 R_A; Table S1 in Supporting Information S1) plot in the canonical range of crustal $^3He/^4He$ (0.01−0.05 R_A; Ballentine et al., 2002) and have <0.5% mantle He inputs (Figure 2). This resembles crustal degassing in the adjacent western Himalayas and western Lhasa block (Figure 2). Note that Samples ZGG04, ZGZ08, and ZZB09 (Klemperer et al., 2022) in the western Lhasa block have 1.1−2.1% mantle He inputs (Figure 3a) but are far away from the KKF (~150−300 km; Figure 1a). We do not expect any fluid connections between the KKF and these distant thermal springs; and indeed, Klemperer et al. (2022) attributed the ~1−2% mantle He inputs to the release of primordial ^3He from asthenospheric mantle wedge.

New He isotope data show that geothermal fields on the Gar and Menshi-Kailas segments, as well as the Langjiu geothermal field off the KKF, are characterized by degassing of crustal fluids (Figure 2 and Figure 3a). As mentioned in the Introduction, previous studies (Hoke et al., 2000; Klemperer et al., 2013, 2022; Zhao et al., 2002) identified mantle He degassing at Menshi and Langjiu (Figure 1). Notably, those samples with mantle He inputs (3.5−28% at Menshi and 2.1−3.1% at Langjiu) were collected in the 1990s, while the post-2015 samples [i.e., 2021 and 2022 at Menshi and Langjiu (this study); 2017 at Menshi and Langjiu (S. Klemperer, personal communication); 2015 and 2019 at Langjiu (Sun et al., 2023)] collectively provide unambiguous evidence for crustal degassing (Figure S1 in Supporting Information S1). Such contrasting results from the same geothermal fields, although not strictly the same sample locality, are intriguing and could be attributed to complex subsurface fluid pathways that are able to cause vastly different dilutions of mantle volatiles by crustal fluids. For example, complex gas-water-rock interaction (e.g., subsurface calcite precipitation; Chiodini et al., 2015) could influence the connectivity and permeability of fluid pathways across short length-scales, and on time-scales of only a few years one conduit may become calcified and another conduit may open. This could increase the residence time of mantle fluids in the crust and thus lead to high possibility of crustal He contamination. Further information on the origin of hydrothermal fluids could contribute to our understanding of the controlling factors for He degassing from the KKF.

3.2. Identification of A Crustal ^{4}He-Rich Fluid Reservoir

Hydrothermal gases from the KKF are enriched in either CO_2 or N_2, or both of them (Table S1 in Supporting Information S1). These major gases, together with water, serve as the carrier for He migration through the crust (Hong et al., 2010; O'Nions & Oxburgh, 1988). When arriving at the surface, the thermal spring gases are expected to contain variable amounts of

major and trace gases due to their solubility (*S*) difference in water (Barry et al., 2013). We find that He contents vary significantly from several parts per million by volume (ppmv) to as high as ~1.0−1.6 vol.% (Table S1 and Data Set S1 in Supporting Information S1). About half of the geothermal fields (9 out of 17) on and off the KKF have average He content higher than economic threshold value (~1000 ppmv; Chen et al., 2023) for He resource exploration. Unlike the 1990s Menshi and Langjiu samples (Hoke et al., 2000; Klemperer et al., 2013), new observations in this century show that the KKF is overwhelmingly dominated by crustal degassing [$^{3}He/^{4}He = 0.029 \pm 0.016\ R_A$ (1σ, $n = 50$)]. Taken together, it is reasonable to infer that there is a crustal ^{4}He-rich fluid reservoir in the hydrothermal systems beneath the KKF (Figure 3a).

Spatially, the crustal He degassing is generally focused in a ~30-km-wide zone along the KKF, with He contents decreasing toward more distant regions in the NE and SW, respectively (Figure S2 in Supporting Information S1), suggesting that the KKF is a primary conduit for the uprising and degassing of crustal ^{4}He-rich fluids. Temporally, except for the 1990s Menshi and Langjiu samples, mantle fluid inputs to the hydrothermal systems were not observed throughout the KKF (Figure 3a). One possibility is that the uprising mantle fluids, if any, could be entirely contaminated by the crustal ^{4}He-rich fluid reservoir as mentioned above. The impulsive nature of crustal He degassing has been highlighted for tectonically active regions (Caracausi et al., 2022), which is particularly affected by earthquake events or cycles (Buttitta et al., 2020). We compiled 54 earthquakes (M = 3.2–5.6, average hypocentral depth = ~32 km, time interval = 1990–2022) that occurred on the KKF and in adjacent areas ±50 km off the KKF (Data Set S2 in Supporting Information S1). A prominent peak in earthquake frequency between 2002 and 2004 is observed, and those occurred since 2000 forms an earthquake cluster in the Menshi-Kailas segment (Figure

S3 in Supporting Information S1). Although the KKF may be seismically less active (e.g., number of recorded earthquakes is small; Chevalier, 2019) than many other strike-slip faults such as the Xianshuihe fault (Liu et al., 2023), the increased earthquakes and their clustering in the Menshi-Kailas segment could result in enhanced release of crustal He (Buttitta et al., 2020; Caracausi et al., 2022) and complex changes in subsurface structural conditions (e.g., the closure and opening of fluid conduits), which may have made it difficult to detect mantle He inputs in the post-2015 samples at Menshi and Langjiu.

Many continental strike-slip faults worldwide, such as the San Andreas fault (Kennedy et al., 1997; Kulongoski et al., 2013), the North Anatolia fault (de Leeuw et al., 2010; Güleç et al., 2002), and the Xianshuihe fault (Liu et al., 2023; Zhang et al., 2021b), are characterized by mantle ^{3}He degassing in long time series and thus plausible fluid connections to the mantle. In this respect, the available data from the KKF are insufficient to assess mantle-to-crust fluid connections and the possible impulsive nature of crustal degassing, which requires continuous $^{3}He/^{4}He$ monitoring of thermal springs and further integration with seismic data analysis and geophysical detections of the underlying structures.

3.3. Carbon Origins and Secondary Hydrothermal Processes

Because CO_2 is a major carrier for He and mantle fluids are negligible in the He inventory, carbon origins in hydrothermal systems are expected to be controlled by decarbonation of crustal materials (rather than the mantle), including the reduced and oxidized carbon species (Figure 3b; e.g., organic matter and carbonate rocks). Following separation from the original reservoir, the transport of CO_2-rich fluids to the surface is always accompanied by secondary processes such as solubility-controlled gas-water-rock interaction, calcite precipitation,

and fluid addition from other sources (Buttitta et al., 2023; Randazzo et al., 2022; Ray et al., 2009; Van Soest et al., 1998).

The positive correlation between CO_2/N_2 and $CO_2/^4He$ ratios indicates that N_2-rich gases (roughly differing from the CO_2-rich gases by CO_2/N_2 <2−3; Figure S4a in Supporting Information S1) tend to have lower $CO_2/^4He$ ratios. Particularly, average He content (5961 ppmv) of the N_2-rich gases is ~10 times that of the CO_2-rich gases (523 ppmv; Figure S4b in Supporting Information S1). The preferential dissolution of CO_2 in groundwater could enrich the exsolved gases with high amounts of less soluble species such as N_2 and noble gases (Rizzo et al., 2019). Such selective gas dissolution in groundwater is plausible to explain the $CO_2/^4He$ decrease in the He- and N_2-rich gases (Figure 3c). Moreover, the sequestration of dissolved inorganic carbon as carbonate minerals (e.g., calcite) could also lower $CO_2/^4He$ ratios of residual gas and fluid phases (Barry et al., 2020; Ray et al., 2009), which simultaneously leads to $\delta^{13}C$ variations depending on temperature and pH of the spring water (Gilfillan et al., 2009; Hilton et al., 1998). Modeling results show that calcite precipitation probably occurred at temperatures of ~90−170 ^oC (Figure 3d), or within an expected pH of 6−8 (Gilfillan et al., 2009). Assuming a geothermal gradient of 30 $^oC\ km^{-1}$ for the western Tibet, carbonate minerals may start to precipitate at ~5−6 km depth, consistent with groundwater circulation of the KKF (Wang et al., 2022). The possibility of calcite precipitation is supported by travertine surrounding spring mouths and calcite veins in exhumed fault rocks (Wallis et al., 2013). In contrast, the increasing $CO_2/^4He$ with decreasing He may result from hydrothermal degassing (Figure 3c), which preferentially retains CO_2 over He in the residual fluid phase (i.e., $S_{He} \ll S_{CO2}$ in aqueous fluids; Barry et al., 2014). Furthermore, CO_2 addition into the uprising hydrothermal fluids is also likely because a mixture of crustal reduced

and oxidized carbon could provide CO_2-rich fluids for mixing with those derived from the crustal ^{4}He-rich fluid reservoir (Figure 3d).

3.4. He-CO_2 Mobilization Related to Crustal-Scale Active Deformation

Continental strike-slip faults are important conduits for the outgassing of deeply-sourced volatiles such as He and CO_2 (Kim et al., 2020; Kulongoski et al., 2013; Xu et al., 2022; Zhang et al., 2021b). A crustal ^{4}He- and CO_2-rich fluid reservoir is proposed to sustain the prevailing crustal degassing through the KKF (Figure 4). The formation of such ^{4}He- and CO_2-rich fluid reservoir depends on (i) liberation of He and CO_2 from variable sources by physical and chemical processes, and (ii) their accumulation in the fluid reservoir as dissolved and gaseous phases (Ballentine et al., 2002). Considering geological and structural features of the KKF, we suggest that the mechanism that could mobilize He and CO_2 from crustal rocks is closely related to active deformation driven by the Karakoram strike-slip faulting (Figure 4).

Strike-slip faults could offset the brittle upper crust and yield at depth to broadly distributed shearing beneath the brittle-ductile transition zone (Figure 4). For the shear zone rocks, dilatancy-related microscale fracturation could enhance the release of crustal ^{4}He into pore fluids (Caracausi et al., 2022). Moreover, deformation-enhanced fault permeability could facilitate fluid infiltration into the carbon-bearing rocks, which thus increases the efficiency of metamorphic decarbonation reactions (Stewart et al., 2019). Therefore, the deforming and fracturing rocks in the ductile shear zone could release large amounts of crustal He and CO_2, which subsequently migrate through the highly fractured fault zones into the hydrothermal system and accumulate over time to form a ^{4}He- and CO_2-rich fluid reservoir. At shallower depths, water-rock interaction and mixing with shallow fluids (e.g., meteoric water infiltrating sediments; Buttitta et al., 2023) could also contribute to the He-CO_2 inventory (Figure 4).

Overall, our model based on geochemical evidence agrees well with geological and geophysical studies that suggest crustal-level localization and thus crustal-scale deformation of the KKF (Craig et al., 2012; Gao et al., 2016; Searle & Phillips, 2007; Van Buer et al., 2015; Wang & Klemperer, 2021).

4. Conclusions

This study presents an attempt to locate the penetration depth and active deformation of continental strike-slip faults based on chemical and isotopic compositions of hydrothermal gases. Our main finding is the crustal ^{4}He- and CO_2-rich fluid reservoir in the subsurface hydrothermal system, which sustains the prevailing crustal degassing from the southern KKF. The failure of the post-2015 measurements in identifying mantle fluids at Menshi and Langjiu may result from (i) complex subsurface fluid conduits that could be changed by hydrothermal processes (e.g., calcite precipitation) and regional seismicity, and (ii) the earthquake cluster in the Menshi-Kailas segment since 2000. Specifically, the former increases the possibility of mantle fluids being diluted by the crustal ^{4}He- and CO_2-rich fluids, while the latter enhances the liberation of crustal ^{4}He and CO_2 from deforming and fracturing fault zone rocks. Although more data are required to evaluate the mantle-to-crust fluid connections and possible impulsive nature of crustal degassing, crustal-scale active deformation is evidently a fundamental response to strike-slip faulting of the southern KKF. Our results provide new geochemical evidence for the penetration depth and active deformation of the KKF, which would be enlightening for interpreting active formation driven by continental strike-slip faults in global orogenic belts.

Acknowledgments

This work was supported by National Natural Science Foundation of China (NSFC) (41930642) and National Key Research and Development Program of China (2020YFA0607700). MZ acknowledges an NSFC grant 42072327. We are grateful to Prof. Simon L. Klemperer and an anonymous reviewer for their constructive and insightful comments that have significantly improved the quality of this manuscript.

Open Research

Data supporting the findings of this study are available at Zhang (2023) https://doi.org/10.5281/zenodo.10297762.

References

Andrews, J. N. (1985). The isotopic composition of radiogenic helium and its use to study groundwater movement in confined aquifers. *Chemical Geology*, *49*(1), 339–351. https://doi.org/10.1016/0009-2541(85)90166-4

Bai, Y., Shi, Z., Zhou, X., Wu, C., Wang, G., He, M., et al. (2023). Gas geochemical evidence for the India-Asia lithospheric transition boundary near the Karakorum fault in western Tibet. *Chemical Geology*, *639*, 121728. https://doi.org/10.1016/j.chemgeo.2023.121728

Ballentine, C. J., Burgess, R., & Marty, B. (2002). Tracing fluid origin, transport and interaction in the crust. *Reviews in Mineralogy and Geochemistry*, *47*(1), 539–614. https://doi.org/10.2138/rmg.2002.47.13

Barry, P. H., Hilton, D. R., Füri, E., Halldórsson, S. A., & Grönvold, K. (2014). Carbon isotope and abundance systematics of Icelandic geothermal gases, fluids and subglacial basalts

with implications for mantle plume-related CO_2 fluxes. *Geochimica et Cosmochimica Acta*, *134*, 74–99. http://doi.org/10.1016/j.gca.2014.02.038

Barry, P. H., Hilton, D. R., Fischer, T. P., de Moor, J. M., Mangasini, F., & Ramirez, C. (2013). Helium and carbon isotope systematics of cold "mazuku" CO_2 vents and hydrothermal gases and fluids from Rungwe Volcanic Province, southern Tanzania. *Chemical Geology*, *339*, 141–156. http://doi.org/10.1016/j.chemgeo.2012.07.003

Barry, P. H., Negrete-Aranda, R., Spelz, R. M., Seltzer, A. M., Bekaert, D. V., Virrueta, C., & Kulongoski, J. T. (2020). Volatile sources, sinks and pathways: A helium-carbon isotope study of Baja California fluids and gases. *Chemical Geology*, *550*, 119722. https://doi.org/10.1016/j.chemgeo.2020.119722

Bourne, S. J., England, P. C., & Parsons, B. (1998). The motion of crustal blocks driven by flow of the lower lithosphere and implications for slip rates of continental strike-slip faults. *Nature*, *391*(6668), 655–659. https://doi.org/10.1038/35556

Buttitta, D., Caracausi, A., Chiaraluce, L., Favara, R., Gasparo Morticelli, M., & Sulli, A. (2020). Continental degassing of helium in an active tectonic setting (northern Italy): the role of seismicity. *Scientific Reports*, *10*(1), 162. https://doi.org/10.1038/s41598-019-55678-7

Buttitta, D., Capasso, G., Paternoster, M., Barberio, M. D., Gori, F., Petitta, M., et al. (2023). Regulation of deep carbon degassing by gas-rock-water interactions in a seismic region of Southern Italy. *Science of the Total Environment*, *897*, 165367. https://doi.org/10.1016/j.scitotenv.2023.165367

Caracausi, A., Buttitta, D., Picozzi, M., Paternoster, M., & Stabile, T. A. (2022). Earthquakes control the impulsive nature of crustal helium degassing to the atmosphere.

Communications Earth & Environment, *3*(1), 224. https://doi.org/10.1038/s43247-022-00549-9

Chen, B., Liu, Y., Fang, L., Xu, S., Stuart, F. M., & Liu, C. (2023). A review of noble gas geochemistry in natural gas from sedimentary basins in China. *Journal of Asian Earth Sciences*, *246*, 105578. https://doi.org/10.1016/j.jseaes.2023.105578

Chevalier, M.-L. (2019). Active tectonics along the Karakorum fault, western Tibetan Plateau: A review. *Acta Geoscientica Sinica*, *40*(1), 37–54. https://doi.org/10.3975/cagsb.2018.101601

Chevalier, M.-L., Van der Woerd, J., Tapponnier, P., Li, H., Ryerson, F. J., & Finkel, R. C. (2015). Late Quaternary slip-rate along the central Bangong-Chaxikang segment of the Karakorum fault, western Tibet. *Geological Society of America Bulletin*, *128*(1–2), 284–314. https://doi.org/10.1130/B31269.1

Chiodini, G., Pappalardo, L., Aiuppa, A., & Caliro, S. (2015). The geological CO_2 degassing history of a long-lived caldera. *Geology*, *43*(9), 767–770. https://doi.org/10.1130/g36905.1

Copley, A., Avouac, J.-P., & Wernicke, B. P. (2011). Evidence for mechanical coupling and strong Indian lower crust beneath southern Tibet. *Nature*, *472*(7341), 79–81. http://doi.org/10.1038/nature09926

Craig, H., Lupton, J., & Horibe, Y. (1978). A mantle helium component in circum-Pacific volcanic gases: Hakone, the Marianas, and Mt. Lassen, in *Advances in Earth and Planetary Science Terrestrial Rare Gases*, edited by E. C. Alexander & M. Ozima, pp. 3-16, Academic publication, Japan

Craig, T. J., Copley, A., & Jackson, J. (2012). Thermal and tectonic consequences of India underthrusting Tibet. *Earth and Planetary Science Letters*, *353–354*, 231–239. https://doi.org/10.1016/j.epsl.2012.07.010

Crossey, L. J., Karlstrom, K. E., Springer, A. E., Newell, D., Hilton, D. R., & Fischer, T. (2009). Degassing of mantle-derived CO_2 and He from springs in the southern Colorado Plateau region—Neotectonic connections and implications for groundwater systems. *Geological Society of America Bulletin*, *121*(7–8), 1034–1053. https://doi.org/10.1130/b26394.1

Day, J. M. D., Barry, P. H., Hilton, D. R., Burgess, R., Pearson, D. G., & Taylor, L. A. (2015). The helium flux from the continents and ubiquity of low-$^3He/^4He$ recycled crust and lithosphere. *Geochimica et Cosmochimica Acta*, *153*, 116–133. https://doi.org/10.1016/j.gca.2015.01.008

de Leeuw, G. A. M., Hilton, D. R., Güleç, N., & Mutlu, H. (2010). Regional and temporal variations in $CO_2/^3He$, $^3He/^4He$ and $\delta^{13}C$ along the North Anatolian Fault Zone, Turkey. *Applied Geochemistry*, *25*(4), 524–539. https://doi.org/10.1016/j.apgeochem.2010.01.010

Ding, L., Kapp, P., Cai, F., Garzione, C. N., Xiong, Z., Wang, H., & Wang, C. (2022). Timing and mechanisms of Tibetan Plateau uplift. *Nature Reviews Earth & Environment*, *3*, 652–667. https://doi.org/10.1038/s43017-022-00318-4

Gao, R., Lu, Z., Klemperer, S. L., Wang, H., Dong, S., Li, W., & Li, H. (2016). Crustal-scale duplexing beneath the Yarlung Zangbo suture in the western Himalaya. *Nature Geoscience*, *9*, 555–560. http://doi.org/10.1038/ngeo2730

Gilfillan, S. M. V., Lollar, B. S., Holland, G., Blagburn, D., Stevens, S., Schoell, M., et al. (2009). Solubility trapping in formation water as dominant CO_2 sink in natural gas fields. *Nature*, *458*(7238), 614–618. https://doi.org/10.1038/nature07852

Graham, D. W. (2002). Noble gas isotope geochemistry of mid-ocean ridge and ocean island basalts: Characterization of mantle source reservoirs. *Reviews in Mineralogy and Geochemistry*, *47*, 247–319. https://doi.org/10.2138/rmg.2002.47.8

Güleç, N., Hilton, D. R., & Mutlu, H. (2002). Helium isotope variations in Turkey: relationship to tectonics, volcanism and recent seismic activities. *Chemical Geology*, *187*(1–2), 129–142. https://doi.org/10.1016/s0009-2541(02)00015-3

Hilton, D. R., McMurtry, G. M., & Goff, F. (1998). Large variations in vent fluid $CO_2/^3He$ ratios signal rapid changes in magma chemistry at Loihi seamount, Hawaii. *Nature*, *396*, 359–362. http://doi.org/10.1038/24603

Hoke, L., Lamb, S., Hilton, D. R., & Poreda, R. J. (2000). Southern limit of mantle-derived geothermal helium emissions in Tibet: Implications for lithospheric structure. *Earth and Planetary Science Letters*, *180*(3–4), 297–308. https://doi.org/10.1016/S0012-821X(00)00174-6

Hong, W.-L., Yang, T. F., Walia, V., Lin, S.-J., Fu, C.-C., Chen, Y.-G., et al. (2010). Nitrogen as the carrier gas for helium emission along an active fault in NW Taiwan. *Applied Geochemistry*, *25*(4), 593–601. https://doi.org/10.1016/j.apgeochem.2010.01.016

Kennedy, B. M., Kharaka, Y. K., Evans, W. C., Ellwood, A., DePaolo, D. J., Thordsen, J., et al. (1997). Mantle fluids in the San Andreas fault system, California. *Science*, *278*(5341), 1278–1281. http://doi.org/10.1126/science.278.5341.1278

Kim, H., Lee, H., Lee, J., Lee, H. A., Woo, N. C., Lee, Y.-S., et al. (2020). Mantle-derived helium emission near the Pohang EGS Site, South Korea: Implications for active fault distribution. *Geofluids*, *2020*, 2359740. https://doi.org/10.1155/2020/2359740

Klemperer, S. L., Kennedy, B. M., Sastry, S. R., Makovsky, Y., Harinarayana, T., & Leech, M. L. (2013). Mantle fluids in the Karakoram fault: Helium isotope evidence. *Earth and Planetary Science Letters*, *366*, 59–70. https://doi.org/10.1016/j.epsl.2013.01.013

Klemperer, S. L., Zhao, P., Whyte, C. J., Darrah, T. H., Crossey, L. J., Karlstrom, K. E., et al. (2022). Limited underthrusting of India below Tibet: $^{3}He/^{4}He$ analysis of thermal springs locates the mantle suture in continental collision. *Proceedings of the National Academy of Sciences*, *119*(12), e2113877119. https://doi.org/10.1073/pnas.2113877119

Kulongoski, J. T., Hilton, D. R., Barry, P. H., Esser, B. K., Hillegonds, D., & Belitz, K. (2013). Volatile fluxes through the Big Bend section of the San Andreas Fault, California: Helium and carbon-dioxide systematics. *Chemical Geology*, *339*, 92–102. https://doi.org/10.1016/j.chemgeo.2012.09.007

Leech, M. L. (2008). Does the Karakoram fault interrupt mid-crustal channel flow in the western Himalaya? *Earth and Planetary Science Letters*, *276*(3), 314–322. https://doi.org/10.1016/j.epsl.2008.10.006

Liu, W., Zhang, M., Chen, B., Liu, Y., Cao, C., Xu, W., et al. (2023). Hydrothermal He and CO_2 degassing from a Y-shaped active fault system in eastern Tibetan Plateau with implications for seismogenic processes. *Journal of Hydrology*, *620*, 129482. https://doi.org/10.1016/j.jhydrol.2023.129482

O'Nions, R. K., & Oxburgh, E. R. (1988). Helium, volatile fluxes and the development of continental crust. *Earth and Planetary Science Letters*, *90*, 331–347. https://doi.org/10.1016/0012-821X(88)90134-3

Randazzo, P., Caracausi, A., Aiuppa, A., Cardellini, C., Chiodini, G., Apollaro, C., et al. (2022). Active degassing of crustal CO_2 in areas of tectonic collision: A case study from the Pollino and Calabria sectors (Southern Italy). *Frontiers in Earth Science*, *10*, 946707. https://doi.org/10.3389/feart.2022.946707

Ray, M. C., Hilton, D. R., Muñoz, J., Fischer, T. P., & Shaw, A. M. (2009). The effects of volatile recycling, degassing and crustal contamination on the helium and carbon geochemistry of hydrothermal fluids from the Southern Volcanic Zone of Chile. *Chemical Geology*, *266*(1–2), 38–49. https://doi.org/10.1016/j.chemgeo.2008.12.026

Rizzo, A. L., Caracausi, A., Chavagnac, V., Nomikou, P., Polymenakou, P. N., Mandalakis, M., et al. (2019). Geochemistry of CO_2-Rich Gases Venting From Submarine Volcanism: The Case of Kolumbo (Hellenic Volcanic Arc, Greece). *Frontiers in Earth Science*, *7*. https://doi.org/10.3389/feart.2019.00060

Robinson, A. C., Owen, L. A., Chen, J., Schoenbohm, L. M., Hedrick, K. A., Blisniuk, K., et al. (2015). No late Quaternary strike-slip motion along the northern Karakoram fault. *Earth and Planetary Science Letters*, *409*, 290–298. https://doi.org/10.1016/j.epsl.2014.11.011

Rosen, M. R., Binda, G., Archer, C., Pozzi, A., Michetti, A. M., & Noble, P. J. (2018). Mechanisms of earthquake-induced chemical and fluid transport to carbonate groundwater springs after earthquakes. *Water Resources Research*, *54*(8), 5225–5244. https://doi.org/10.1029/2017WR022097

448 Royden, L. H., Burchfiel, B. C., & van der Hilst, R. D. (2008). The geological evolution of the
449 Tibetan Plateau. *Science*, *321*(5892), 1054–1058.
450 https://doi.org/10.1126/science.1155371
451 Sano, Y., & Fischer, T. P. (2013). The analysis and interpretation of noble gases in modern
452 hydrothermal systems, in *The Noble Gases as Geochemical Tracers*, edited by P.
453 Burnard, pp. 249–317, Springer, Berlin Heidelberg. http://doi.org/10.1007/978-3-642-
454 28836-4_10
455 Searle, M. P., & Phillips, R. J. (2007). Relationships between right-lateral shear along the
456 Karakoram fault and metamorphism, magmatism, exhumation and uplift: evidence from
457 the K2–Gasherbrum–Pangong ranges, north Pakistan and Ladakh. *Journal of the*
458 *Geological Society*, *164*(2), 439–450. https://doi.org/10.1144/0016-76492006-072
459 Stewart, E. M., Ague, J. J., Ferry, J. M., Schiffries, C. M., Tao, R.-B., Isson, T. T., & Planavsky,
460 N. J. (2019). Carbonation and decarbonation reactions: Implications for planetary
461 habitability. *American Mineralogist*, *104*(10), 1369–1380. https://doi.org/10.2138/am-
462 2019-6884
463 Sun, Y., Guo, Z., Fortin, D., Zhao, W., Cheng, Z., Li, J., & Zhang, Y. (2023). Diffuse emission
464 of CO_2 from the Langjiu Geothermal Field, Western Tibet. *Journal of Geochemical*
465 *Exploration*, *249*, 107219. https://doi.org/10.1016/j.gexplo.2023.107219
466 Sylvester, A. G. (1988). Strike-slip faults. *Geological Society of America Bulletin*, *100*(11),
467 1666–1703. https://doi.org/10.1130/0016-7606(1988)100<1666:SSF>2.3.CO;2
468 Umeda, K., & Ninomiya, A. (2009). Helium isotopes as a tool for detecting concealed active
469 faults. *Geochemistry, Geophysics, Geosystems*, *10*(8), Q08010.
470 https://doi.org/10.1029/2009GC002501

Van Buer, N. J., Jagoutz, O., Upadhyay, R., & Guillong, M. (2015). Mid-crustal detachment beneath western Tibet exhumed where conjugate Karakoram and Longmu–Gozha Co faults intersect. *Earth and Planetary Science Letters*, *413*, 144–157. https://doi.org/10.1016/j.epsl.2014.12.053

Van Soest, M. C., Hilton, D. R., & Kreulen, R. (1998). Tracing crustal and slab contributions to arc magmatism in the Lesser Antilles island arc using helium and carbon relationships in geothermal fluids. *Geochimica et Cosmochimica Acta*, *62*(19–20), 3323–3335. https://doi.org/10.1016/S0016-7037(98)00241-5

Wallis, D., Phillips, R. J., & Lloyd, G. E. (2013). Fault weakening across the frictional-viscous transition zone, Karakoram Fault Zone, NW Himalaya. *Tectonics*, *32*(5), 1227–1246. https://doi.org/10.1002/tect.20076

Wang, J., Zhou, X., He, M., Li, J., Dong, J., Tian, J., et al. (2022). Hydrogeochemical origin and circulation of spring waters along the Karakorum fault, Western Tibetan Plateau: Implications for interaction between hydrosphere and lithosphere. *Frontiers in Earth Science*, *10*, 1021550. https://doi.org/10.3389/feart.2022.1021550

Wang, S., & Klemperer, S. L. (2021). Love-wave normal modes discriminate between upper-mantle and crustal earthquakes: Simulation and demonstration in Tibet. *Earth and Planetary Science Letters*, *571*, 117089. https://doi.org/10.1016/j.epsl.2021.117089

Wright, T. J., Parsons, B., England, P. C., & Fielding, E. J. (2004). InSAR observations of low slip rates on the major faults of western Tibet. *Science*, *305*(5681), 236–239. https://doi.org/10.1126/science.1096388

Xu, S., Guan, L., Zhang, M., Zhong, J., Liu, W., Xie, X. g., et al. (2022). Degassing of deep-sourced CO_2 from Xianshuihe-Anninghe fault zones in the eastern Tibetan Plateau.

Science China Earth Sciences, *65*(1), 139–155. https://doi.org/10.1007/s11430-021-9810-x

Zhang, M. (2023). mzhangrocks/KarakoramFault: Data files for hydrothermal degassing from the Karakoram fault [Data set]. Zenodo. https://doi.org/10.5281/zenodo.10297762

Zhang, M., Xu, S., Zhou, X., Caracausi, A., Sano, Y., Guo, Z., et al. (2021a). Deciphering a mantle degassing transect related with India-Asia continental convergence from the perspective of volatile origin and outgassing. *Geochimica et Cosmochimica Acta*, *310*, 61–78. https://doi.org/10.1016/j.gca.2021.07.010

Zhang, M., Guo, Z., Xu, S., Barry, P. H., Sano, Y., Zhang, L., et al. (2021b). Linking deeply-sourced volatile emissions to plateau growth dynamics in southeastern Tibetan Plateau. *Nature Communications*, *12*(1), 4157. https://doi.org/10.1038/s41467-021-24415-y

Zhao, P., Xie, E., Dor, J., Jin, J., Hu, X., Du, S., & Yao, Z. (2002). Geochemical characteristics of geothermal gases and their geological implications in Tibet. *Acta Petrologica Sinica*, *18*(4), 539–550. (in Chinese with English abstract).

Figure Caption

Figure 1. (a) Map showing geo-tectonic framework and sample locality. Bold italic letters M and L refer to Menshi and Langjiu, respectively. (b) Enlarged map of the southern Karakoram fault. Insert of fault segmentation is after Chevalier et al. (2015). The compiled earthquake events (Data Set S2 in Supporting Information S1) are from USGS Earthquake Catalog.

Figure 2. Plot of $^{3}He/^{4}He$ (R_M/R_A) versus X value. Filled and open symbols represent data in this study and literature, respectively. Air-saturated water (ASW; $^{3}He/^{4}He$ = 0.985 R_A, $^{4}He/^{20}Ne$ =

0.26) is from Klemperer et al. (2022). Mantle end-member refers to a combination of depleted MORB-sourced mantle (8 ± 1 R_A; Graham, 2002) and SCLM (6.1 ± 2.1 R_A; Day et al., 2015). Crust-mantle mixtures with variable mantle proportions, calculated from mixing between MORB-type mantle (8 R_A) and crust (0.02 R_A), are shown for comparison. $^4He/^{20}Ne$ ratio of crust, mantle, and crust-mantle mixtures is assumed to be 3500. Changlung (CL) and Duoguoqu (DGQ) are shown for comparison with the 1990s Menshi and Langjiu samples. The horizontal scale bar represents proportions of ASW-derived He in uncorrected $^3He/^4He$ values.

Figure 3. Plots of He-CO_2 systematics. (a) $^3He/^4He$ (R_C/R_A) versus 1/He. (b) $^3He/^4He$ (R_C/R_A) versus $\delta^{13}C$-CO_2 (‰). (c) $CO_2/^4He$ versus 1/He. (d) $CO_2/^4He$ versus $\delta^{13}C$-CO_2 (‰). Data source and symbols are as in Figure 2. The initially exsolved gases from crustal fluid reservoir are defined according to geochemical tendency of samples. Reference values of end-member parameters are given in Table S2 in Supporting Information S1. Note that in some cases the $\delta^{13}C$-CO_2 value of mantle fluids could be comparable with that of the mixture between crustal reduced and oxidized carbon; however, crustal ^4He-rich fluids are expected to have lower $CO_2/^4He$ than mantle fluids due to excessed ^4He relative to CO_2. Model of calcite precipitation (CP) is after Barry et al. (2020).

Figure 4. Cartoon showing crustal-scale active deformation and related hydrothermal degassing. Groundwater circulation depth is after Wang et al. (2022) and the brittle-ductile transition zone is assumed to be at ~30 km depth for western Tibet.

Figure 1.

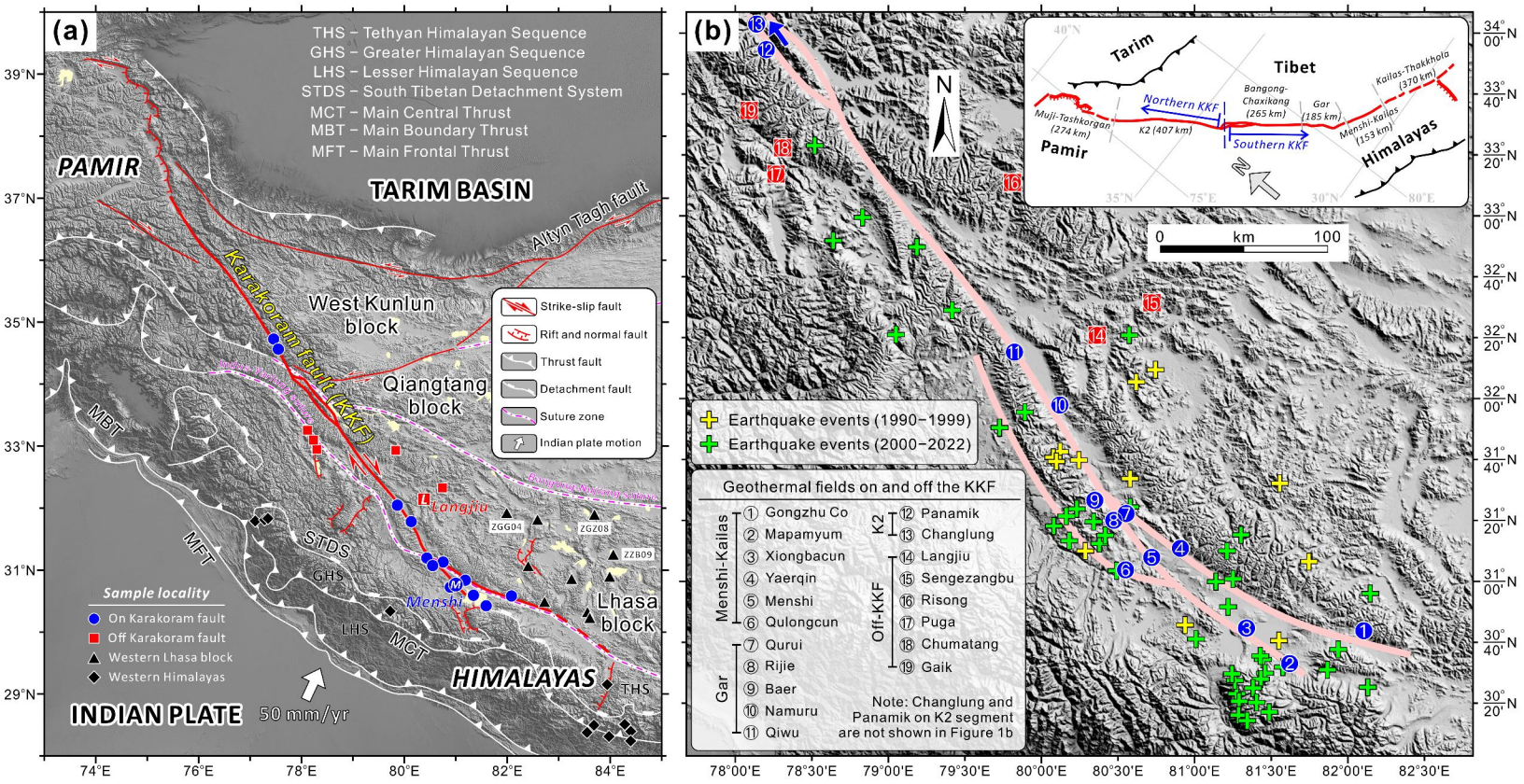
(a)
THS – Tethyan Himalayan Sequence
GHS – Greater Himalayan Sequence
LHS – Lesser Himalayan Sequence
STDS – South Tibetan Detachment System
MCT – Main Central Thrust
MBT – Main Boundary Thrust
MFT – Main Frontal Thrust
PAMIR
TARIM BASIN
Altyn Tagh fault
Karakoram fault (KKF)
West Kunlun block
Qiangtang block
Lhasa block
HIMALAYAS
INDIAN PLATE
50 mm/yr
MBT
MFT
STDS
GHS
LHS
MCT
THS
Langjiu
Menshi
ZGG04
ZGZ08
ZZB09
Strike-slip fault
Rift and normal fault
Thrust fault
Detachment fault
Suture zone
Indian plate motion
Sample locality
On Karakoram fault
Off Karakoram fault
Western Lhasa block
Western Himalayas
39°N
37°N
35°N
33°N
31°N
29°N
74°E
76°E
78°E
80°E
82°E
84°E
(b)
N
Tarim
Tibet
Pamir
Himalayas
Northern KKF
Southern KKF
K2 (407 km)
Muji-Tashkorgan (274 km)
Bangong-Chaxikang (265 km)
Gar (185 km)
Menshi-Kailas (153 km)
Kailas-Thakkhola (370 km)
0 km 100
Earthquake events (1990–1999)
Earthquake events (2000–2022)
Geothermal fields on and off the KKF
Menshi-Kailas
① Gongzhu Co
② Mapamyum
③ Xiongbacun
④ Yaerqin
⑤ Menshi
⑥ Qulongcun
Gar
⑦ Qurui
⑧ Rijie
⑨ Baer
⑩ Namuru
⑪ Qiwu
K2
⑫ Panamik
⑬ Changlung
Off-KKF
⑭ Langjiu
⑮ Sengezangbu
⑯ Risong
⑰ Puga
⑱ Chumatang
⑲ Gaik
Note: Changlung and Panamik on K2 segment are not shown in Figure 1b
34°00'N
33°40'N
33°20'N
33°00'N
32°40'N
32°20'N
32°00'N
31°40'N
31°20'N
31°00'N
30°40'N
30°20'N
78°00'E
78°30'E
79°00'E
79°30'E
80°00'E
80°30'E
81°00'E
81°30'E
82°00'E
82°30'E

Figure 2.

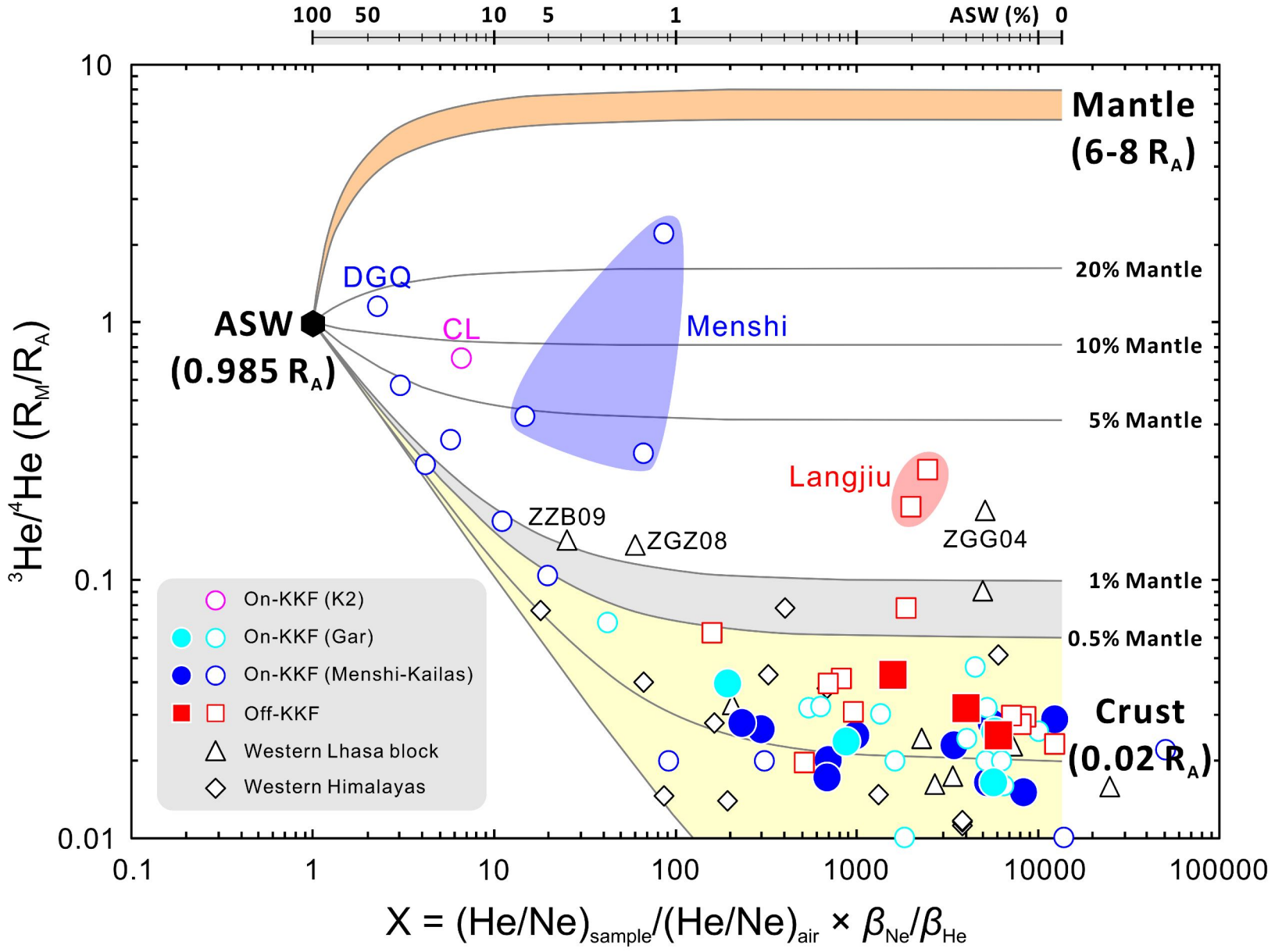
100 50 10 5 1 ASW (%) 0
Mantle
(6-8 R_A)
20% Mantle
10% Mantle
5% Mantle
1% Mantle
0.5% Mantle
Crust
(0.02 R_A)
ASW
(0.985 R_A)
DGQ
CL
Menshi
Langjiu
ZZB09
ZGZ08
ZGG04
On-KKF (K2)
On-KKF (Gar)
On-KKF (Menshi-Kailas)
Off-KKF
Western Lhasa block
Western Himalayas
3He/4He (RM/RA)
10
1
0.1
0.01
0.1
1
10
100
1000
10000
100000
X = (He/Ne)sample/(He/Ne)air × βNe/βHe

Figure 3.

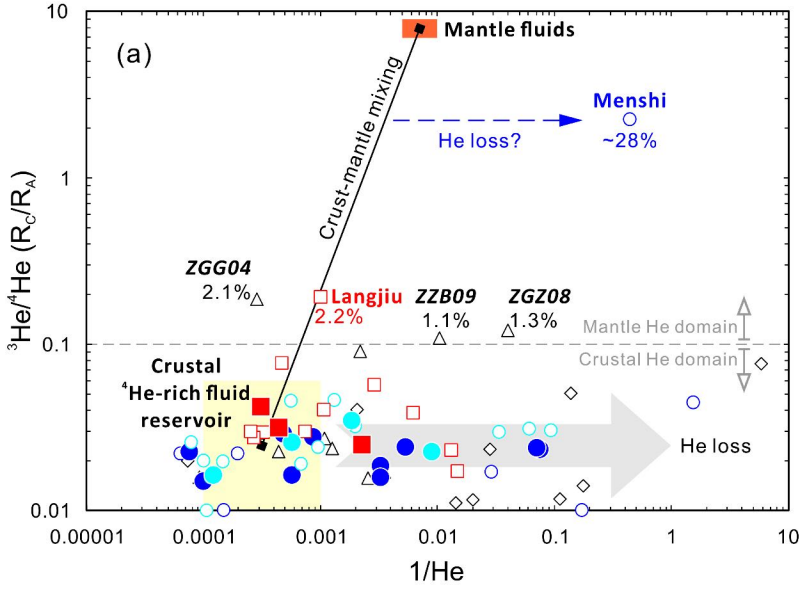
(a)
Mantle fluids
Crust-mantle mixing
Menshi
He loss?
~28%
ZGG04
2.1%
Langjiu
2.2%
ZZB09
1.1%
ZGZ08
1.3%
Mantle He domain
Crustal He domain
Crustal
4He-rich fluid
reservoir
He loss
3He/4He (RC/RA)
1/He

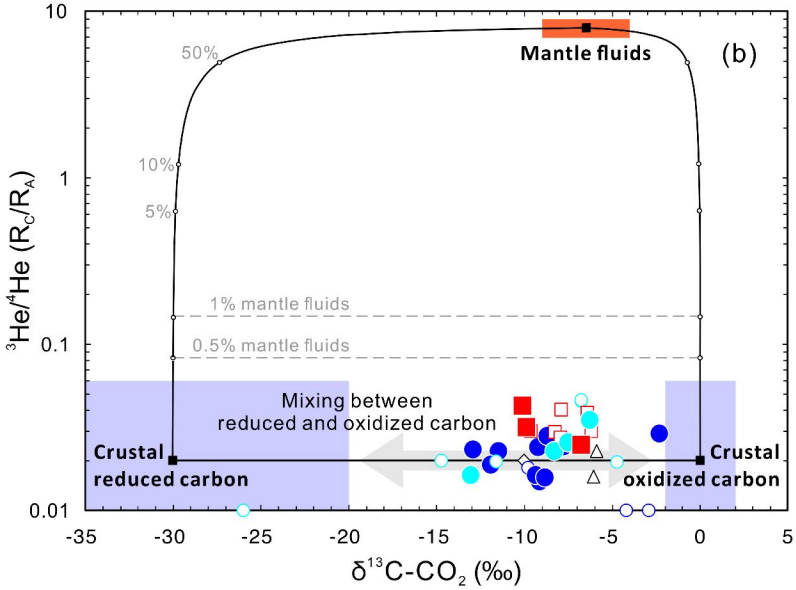
(b)
Mantle fluids
50%
10%
5%
1% mantle fluids
0.5% mantle fluids
Mixing between
reduced and oxidized carbon
Crustal
reduced carbon
Crustal
oxidized carbon
3He/4He (RC/RA)
δ13C-CO2 (‰)

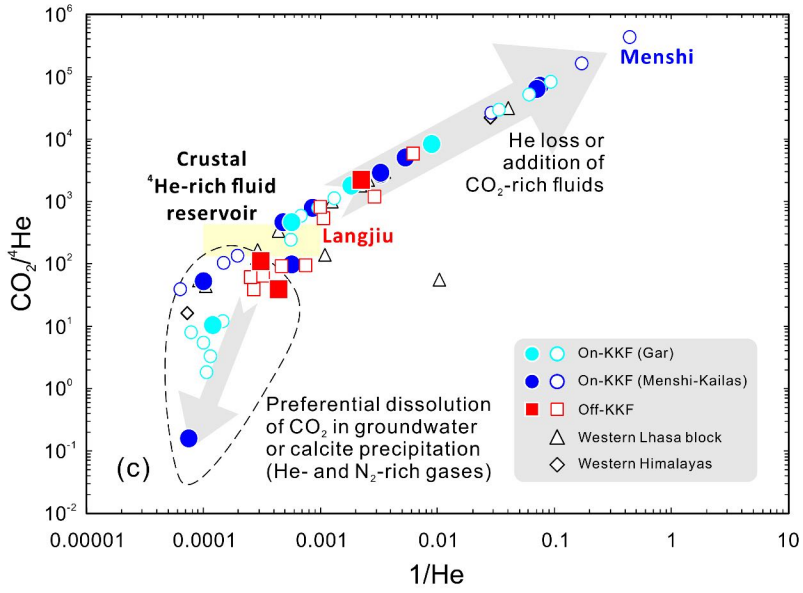
(c)
Menshi
Crustal
4He-rich fluid
reservoir
Langjiu
He loss or
addition of
CO2-rich fluids
Preferential dissolution
of CO2 in groundwater
or calcite precipitation
(He- and N2-rich gases)
On-KKF (Gar)
On-KKF (Menshi-Kailas)
Off-KKF
Western Lhasa block
Western Himalayas
CO2/4He
1/He

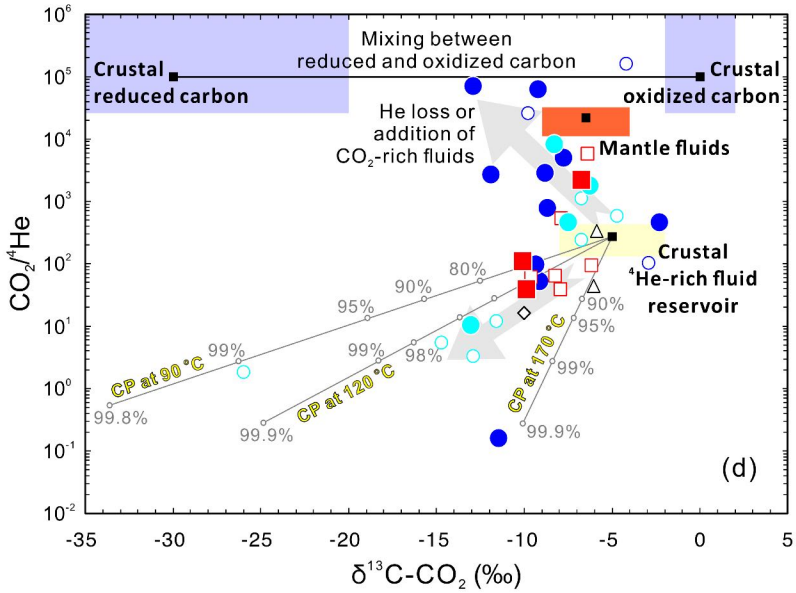
(d)
Mixing between
reduced and oxidized carbon
Crustal
reduced carbon
Crustal
oxidized carbon
He loss or
addition of
CO2-rich fluids
Mantle fluids
Crustal
4He-rich fluid
reservoir
CP at 90 °C
CP at 120 °C
CP at 170 °C
99.8%
99.9%
99.9%
99%
95%
90%
80%
98%
CO2/4He
δ13C-CO2 (‰)

Figure 4.

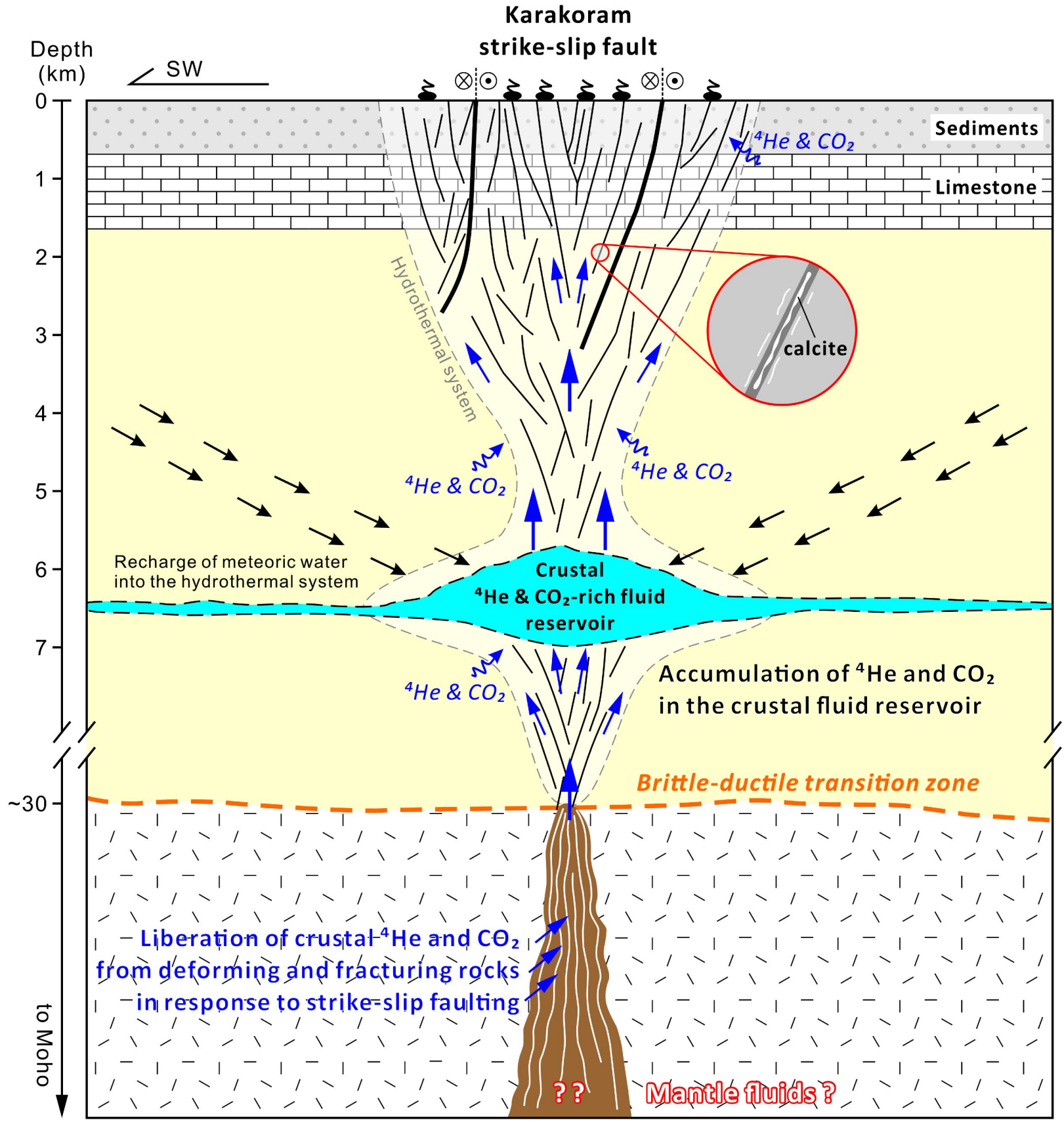
Karakoram
strike-slip fault
Depth
(km)
SW
0
1
2
3
4
5
6
7
~30
to Moho
Sediments
Limestone
^4He & CO_2
Hydrothermal system
calcite
^4He & CO_2
^4He & CO_2
^4He & CO_2
Recharge of meteoric water
into the hydrothermal system
Crustal
^4He & CO_2-rich fluid
reservoir
Accumulation of ^4He and CO_2
in the crustal fluid reservoir
Brittle-ductile transition zone
Liberation of crustal ^4He and CO_2
from deforming and fracturing rocks
in response to strike-slip faulting
??
Mantle fluids ?